Journal of the Australian Ceramic Society (2020) 56:99–108
https://doi.org/10.1007/s41779-019-00398-4

RESEARCH

Production parameters affecting the synthesis and properties of hBN-SiC composites

Zuhal Yılmaz[1] · Nuran Ay[2]

Received: 30 August 2018 / Revised: 27 May 2019 / Accepted: 2 August 2019 / Published online: 16 January 2020

Abstract

In this study, the hexagonal boron nitride (hBN)-SiC composite powder synthesis was investigated with an in situ reaction method. Boric acid (H_3BO_3) and urea ($CO(NH_2)_2$) were used for hBN formation. In the hBN-SiC composite powder synthesis, primarily raw materials were homogeneously stirred in ethanol with Si_3N_4 balls. The samples were calcined and sintered by spark plasma sintering at 2000 °C under pressure of 50 MPa for 15 min. The characterization of composite samples was carried out by XRD, SEM-EDS, FTIR, and TG-DTA. The bulk density, Vickers hardness, and Young's modulus of samples were also measured. Composites were obtained, which had homogeneous microstructure. Residual boron oxides were found in samples with short calcination times. Moreover, it was found that the production parameters affect the physical properties of the composites and the amount of the hBN in sintered samples.

Keywords hBN · SiC · Composites · Calcination · Physical properties

Introduction

Silicon carbide (SiC) is one of the most important ceramic materials due to its high hardness and strength, chemical and thermal stability, high melting point, oxidation resistance, and high wear resistance at high temperatures. Besides its mechanical properties, due to its electronic and semi-conductive properties, it is used in many areas [1–3]. However, SiC ceramics were difficult to be machined for complex component engineering applications. Hexagonal boron nitride (hBN) is an inorganic material that finds many application possibilities in the industry with its properties such as its carbon-like crystal structure, high thermal shock resistance, thermal conductivity, electrical insulation, chemical stability, lubricity, and machinability [4, 5]. It is shown that the machinability of ceramic materials increases with the addition of hBN, while the machinability of SiC has been improved by the addition of micron-sized hBN powder; also, it has been reported that the mechanical properties of hBN-SiC were significantly reduced [6, 7]. Furthermore, in situ processes could create finer and more homogeneous microstructures that have higher chemical and microstructural stability and better mechanical properties than those obtained by conventional processes [8]. hBN-SiC composites were synthesized by an in situ method using several raw materials, for example, Si_3N_4, B_4C, and C [8–11]; Si_3N_4, H_3BO_3, and C [12]; B_4C and Si powder [13]; and SiO_2, H_3BO_3, and C [14].

Urea ($CO(NH_2)_2$) is an inexpensive, non-toxic chemical that can decompose in environments with water according to reaction (1) to yield the actual reducing agent NH_3. The industrial production of NH_3 from urea is a widely used process.

$$CO(NH_2)_2 + H_2O \rightarrow 2NH_3(g) + CO_2(g) \quad (1)$$

hBN-SiC composites were obtained by utilizing urea as raw material. Although there are other studies which employed urea as raw material, the calcination temperatures, times, and sintering methods (hot press, reactive hot pressing, applying an electric current in a high-pressure combustion reactor, etc.) were different in these studies [6, 7, 15–17]. In some studies, hBN-SiC nanocomposites were calcined at 850 °C for 16 h in a nitrogen atmosphere [16, 17].

✉ Zuhal Yılmaz
zuhal.guven@bilecik.edu.tr

Nuran Ay
nay@eskisehir.edu.tr

[1] SMYO, Bilecik Şeyh Edebali University, Bilecik, Turkey

[2] Department of Material Science and Engineering, Eskişehir Technical University, Eskişehir, Turkey

Moreover, in the study of Kusunose et al., hBN-SiC nanocomposites were calcined at 350 °C for 3 h and 1100 °C for 8 h in a hydrogen atmosphere [15]. In another study, the calcination temperature of the hBN-SiC nanocomposite was selected as 850 °C for 21 h in a nitrogen atmosphere [6]. Furthermore, in the study of Jin et al., the composite was calcined at 850 °C for 21 h and at 1100 °C for 6 h in a nitrogen atmosphere [7]. According to these studies, it was determined that the first stage in the production of hBN-SiC composites was the calcination process. Also, in these studies, it has not been adequately explained why different temperatures and times were preferred during the calcination process.

In this study, the hBN-SiC composite was synthesized by an in situ method using α-SiC, H_3BO_3, and $CO(NH_2)_2$. The effect of calcination times on the hBN-SiC composite production was investigated at 850 °C for 4, 8, 12, and 16 h, considering the literature studies. Thus, the effects of different calcination times not included in the literature studies on the synthesis and properties of hBN-SiC composites were determined. The calcined composite powders were sintered by spark plasma sintering (SPS) at 2000 °C.

Experimental studies

The starting raw materials, silicon carbide (2 μm, α-SiC) (Alfa Aesar, Germany), boric acid (H_3BO_3) (Merck, Germany), and urea ($CO(NH_2)_2$) (Merck, Germany), were used for producing hBN-SiC composites. In this process, the boric acid and urea (according to the mole ratio 1:3) and silicon carbide were homogeneously mixed in the planetary mill (Fritsch, Pulverisette) in ethanol and with 13-mm-diameter silicon nitride ball and then dried. All of the samples were prepared in a ratio of which theoretically 30 wt% hBN in each sample. After drying, the mixture samples were calcined at 850 °C under a nitrogen atmosphere for 4, 8, 12, and 16 h. The obtained composite powder samples were coded as S3-4, S3-8, S3-12, and S3-16 according to the calcination time. The composite powders were sintered by SPS (HPD-50, FCT GmbH, Germany) at 2000 °C, under a vacuum atmosphere by applying 50 MPa of pressure for 15 min. The composite powders were placed in a graphite die with a 20-mm diameter, heat treated up to 2000 °C with a 100 °C/min heating rate, and the powders were turned off to achieve fast cooling. The electric current was pulsed periodically with 12 pulses/ms (2 of 12 pulses off as a recovery time). The temperature was increased by controlled electrical current and was measured with an optical pyrometer inside the graphite punches. The sintered composite powders were coded as S3-4S, S3-8S, S3-12S, and S3-16S.

Thermal analysis of mixed composite powders and calcined powders was carried out with TG-DTA (Netzsch, STA 449 F3). Thermal analysis was conducted in a nitrogen atmosphere with a 5 °C/min heating rate up to 1400 °C. The crystalline phases of the calcined composite powders and sintered samples were determined using an X-ray diffractometer (XRD). X-ray powder diffraction patterns were obtained with a Rigaku Rint 2000 X-ray diffractometer with CuKα radiation ($\lambda = 1.5418$ Å), in the 2θ range of 20–50° with the scan speed of 2°/min. The amount of the phases was calculated by using the JADE software and MAUD program. The surface morphologies of calcined and sintered samples were investigated by means of scanning electron microscopy (SEM, ZEISS SUPRA 50VP) which is equipped with an energy-dispersive X-ray probe (EDS, Oxford Instruments, UK)). FTIR was recorded with a Bruker Tensor 27 model spectrophotometer within the range 600–4000 cm^{-1}. The density and open porosity were evaluated by Archimedes' principle. The microhardness was tested on a polished surface by Vickers indentation with a load of 5 kg for a 5-s dwell time (EMCO TEST M1C 010).

The theoretical density was calculated using the mass fractions and densities. The density values of SiC and hBN were utilized as 3.21 g/cm^3 and 2.27 g/cm^3, respectively. The B_2O_3 density is not included in the theoretical density calculation. Young's modulus was determined by the non-destructive method with a Tektronix TDS 1012 oscilloscope.

Results and discussion

Thermal analysis

According to the thermal analysis results, the mass loss of the composite powder mixture was completed at ~800 °C (Fig. 1). Urea completes thermal reactions up to about 750 °C and degradation is very slow above this temperature [18]. Urea is transformed into biurea form when it melts at 133 °C, and at the same the mixtures lose water. However, its physical structure is not clear at this temperature, although it is reported to have begun to melt [19, 20]. It has been mentioned that formation of biurea from 133 to 220 °C is continued [19]. Amylin, melamine, ammonia (NH_3), and cyanuric acid $(HNCO)_3$ occur with increasing temperature, and mass change takes place with a decomposition of NH_3 and $(HNCO)_3$ at around 380–400 °C. It has been shown that the formation of carbon, nitrogen, and hydrogen continued up to 700 °C with increasing temperature [18–20]. In the TG-DTA graph of the composite powder mixture, it was pointed out that the peaks of dehydration of boric acid overlap with decomposition peaks of urea. The boric acid loses its water above 150 °C and transforms to boron oxide. Although crystalline boron oxide has a melting point at 450 °C, amorphous boron oxide does not have a specific melting temperature. Amorphous boron oxide begins to melt at 325 °C and becomes fluid at 500 °C [21, 22]. According to these results,

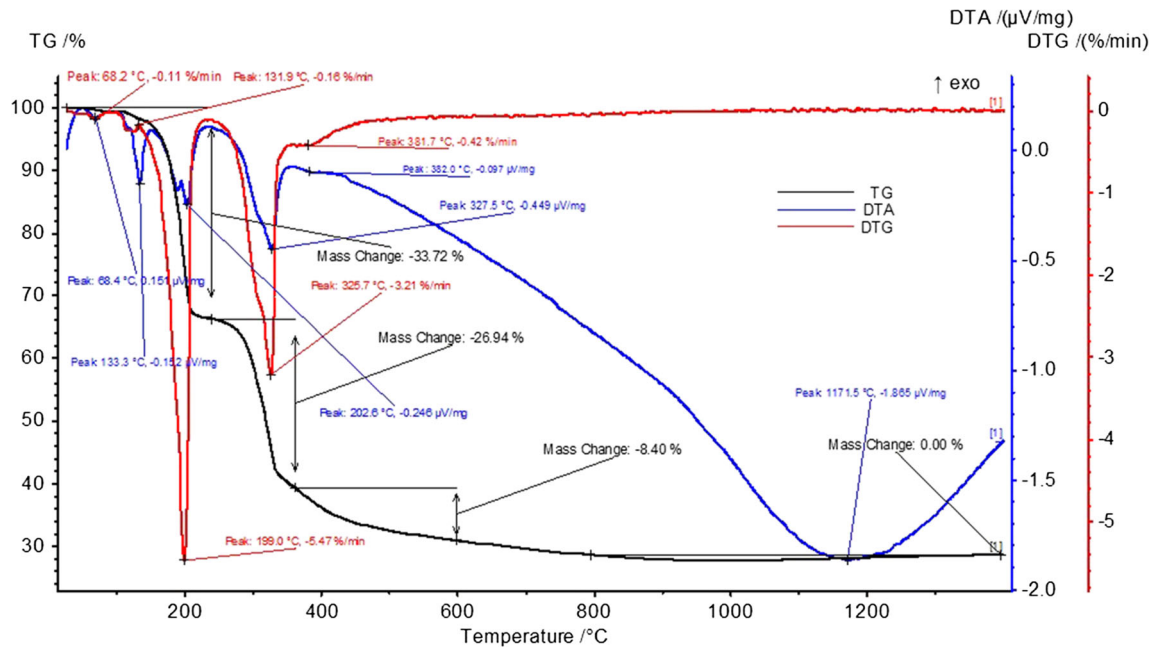

Fig. 1 The thermal analysis for raw composite mixture

the calcination temperature of the samples was selected as 850 °C.

In the thermal analysis results of the calcined samples at 850 °C and in different calcination times, it has been observed that reactions continue and mass loss occurs (Fig. 2). The mass loss of the sample S3-4 was 7.51% (being the highest value among the other samples) that was calcined for 4 h. The mass loss of samples S3-8, S3-12, and S3-16 was 3.34%,

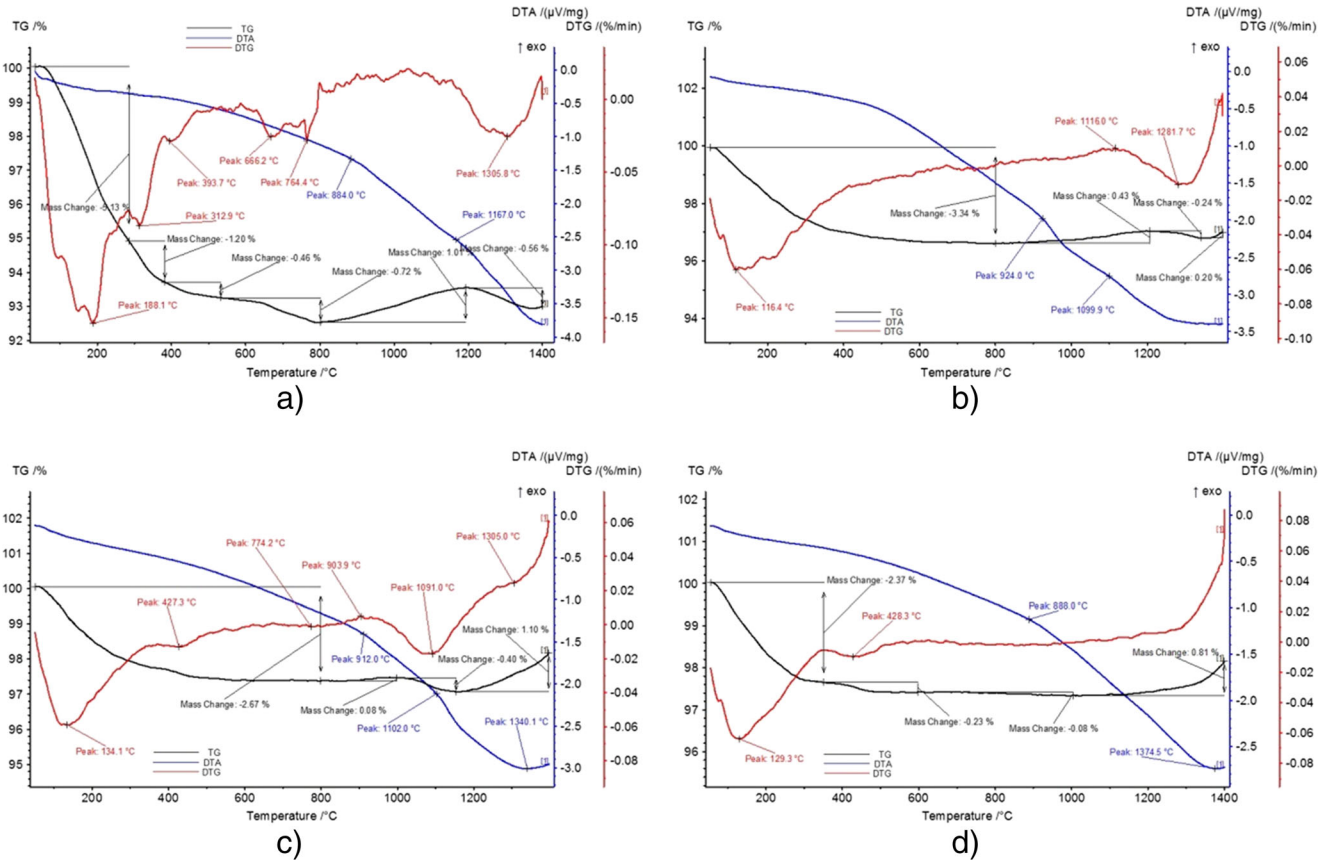

Fig. 2 The thermal analysis graphs of calcined samples at 850 °C. **a** S3-4. **b** S3-8. **c** S3-12. **d** S3-16

2.67%, and 2.68%, respectively. As calcination time increases, mass loss decreases depending upon time. The reason for mass loss in the samples is thought to be that the raw materials still do not complete decomposition or that it is due to the hydration of the composite powders after calcination. It can be said that the urea and boric acid reactions are performed less in the 4-h calcination times. As calcination time is extended, endothermic peaks decrease. There are mass increases above 1000 °C in Fig. 2, and it is thought to be that nitrogen contributes to the formation of BN during the thermal analysis [23].

Characterizations

The FTIR spectrum of calcined samples at 850 °C is demonstrated in Fig. 3. Two strong characteristic peaks are located at 1390–1400 and 790–835 cm^{-1} which could be observed clearly in all samples. The peak at 1390–1400 cm^{-1} can be attributed to the B–N stretching vibrations [24, 25]. The other peak located at 790–835 cm^{-1} is due to the B–N–B bending vibrations and Si–C stretching vibrations. In the literature, the peaks at 800 and 834 cm^{-1} are related to the Si–C vibrations [26, 27]. While there is only a single one peak at 790–835 cm^{-1} in S3-4, the presence of the 2nd peak in S3-8 starts to appear and two peaks are at 790–806 and 829–835 cm^{-1} in S3-12 and S3-16, respectively (Fig. 3). The peak observed at 1100–1106 cm^{-1} is probably because of the presence of some surface bonds containing boron and/or nitrogen, C–B bond [24], or could be referred to B–O–H in-plane vibrations [28]. The intensity of the peak at 1100–1106 cm^{-1} is reduced due to the increase in calcination time. It indicates that boron oxide remains in the system when calcination time decreases. The small peak observed at 680 cm^{-1} is probably due to the Si–H bond [29, 30] or various bonds of B and N with oxygen: B–O, O–B–O, B–O–B, and B–N–O [31]. The peak seen at 1620–1690 cm^{-1} can be attributed to the C=O stretching vibrations [32–35] or could be referred to N–H vibrations [36] in the S3-4 sample. As a result, it points to the presence of urea residues at S3-4. The 2360 cm^{-1} peak is attributed to environmental CO_2 gas [37, 38].

Figure 4 shows the XRD patterns drawn with raw data of the calcined samples for different calcination times. It is found that the calcination time does not affect the SiC phases. BN formation was not observed in the XRD patterns after calcination because it has not completed the formation of hBN structure. However, the FTIR analysis showed the B–N stretching vibrations and the B–N–B bending vibrations. Because this reaction temperature (850 °C) is lower than the conversion temperature of the amorphous boron nitride to the crystalline boron nitride, the composite powders are coated with amorphous boron nitride. Wang et al. measured an amorphous BN cloud thickness of less than 100 nm and a few 20–30-nm size particles at 850 °C [16]. As reported in the literature, hBN formation occurs at temperatures above 1500 °C [39–42]. According to Hubáček et al., boron nitrides are turbostratic when heated to 1300 °C: the mesographitic form of hexagonal boron nitride at between 1300 and 1600 °C and the crystalline hexagonal form at 1600 °C [43]. In the EDS analysis, there are boron, nitrogen, and oxygen peaks in all the calcined samples (Fig. 5). This oxygen is thought to be caused by materials that have not completed the reaction from the precursor materials. Brožek and Hubáček have reported that growth of boron nitride crystals is a condensation character and the termination of it is seen as a reaction of hydroxylic and hydrogen radicals in periphery areas of the macromolecules. This approach can elucidate the formation of a certain amount of oxygen in samples treated even at high temperatures [44]. TG and FTIR results support this approach. Studies on hBN production show that these impurities are removed by washing with HCl [40] or pure water [43] after heat treatment. Because boron nitride is amorphous, it is not observed in the

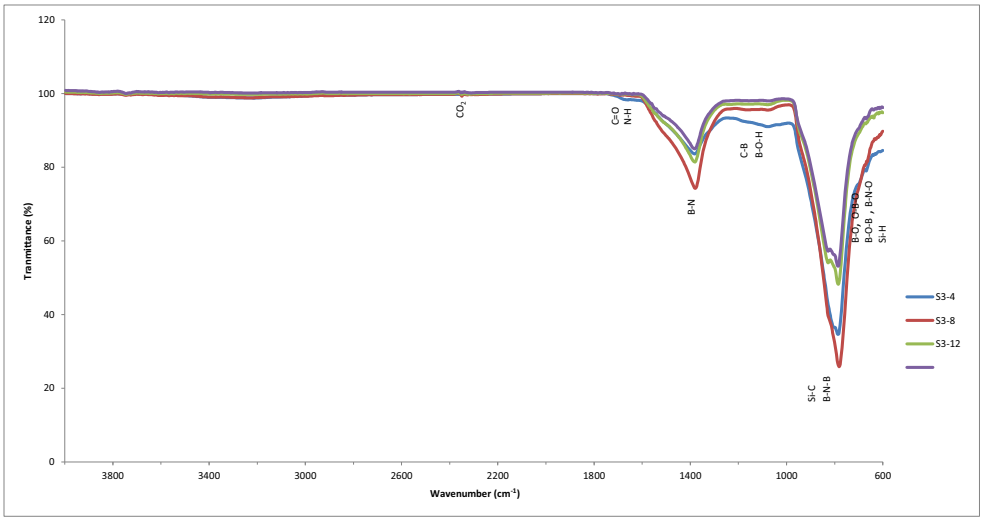

Fig. 3 FTIR analysis spectra of calcined samples at 850 °C cm^{-1}

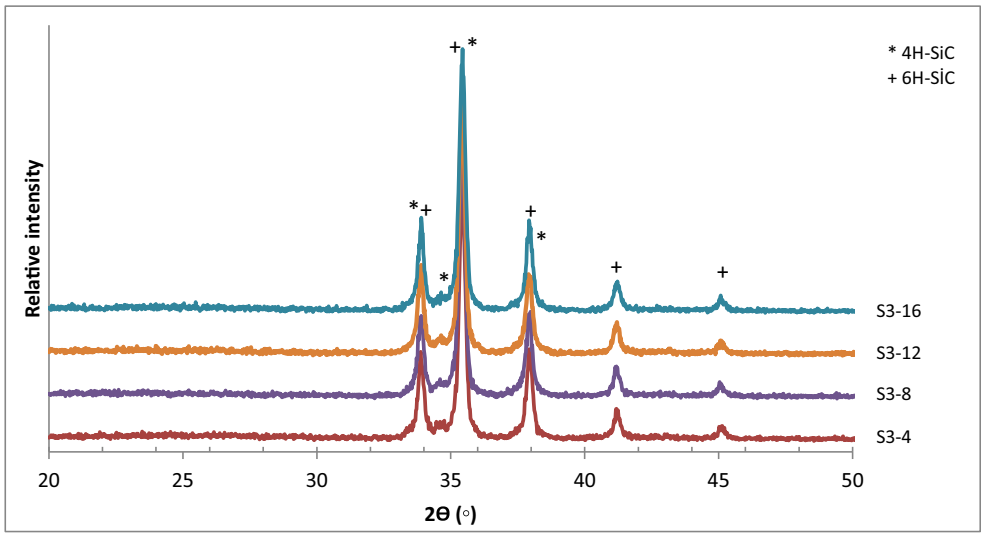

Fig. 4 XRD patterns of the hBN-SiC composite powders after calcination at 850 °C

SEM images of all samples at different calcination times (Fig. 6).

After sintering by SPS at 2000 °C for 15 min under pressure 50 MPa, the hBN (JCPDS PDF no. 034-0421) peaks were detected in all samples (Fig. 7). Boron oxide (JCPDS PDF no. 006-0297) continued to exist in the 4-, 8-, and 12-h calcined and sintered samples. In the 16-h calcined and sintered sample, there is no boron oxide. In the SEM images of all the sintered samples, the hBN particles can be clearly seen (Fig. 8). In the EDS analysis, there are boron and nitrogen peaks in the sample (Fig. 9). The hBN has a flake shape and formed homogeneously at the grain boundaries of SiC [8]. The hBN flakes in all the samples were measured for over 1 μm. For the samples that are calcinated at 850 °C for 16 h and hot pressed at 1850 °C, the hBN particle sizes were reported to be below 100 nm [17]. In some studies, nanometer hBN formation is also mentioned when the samples were subjected to different sintering processes with various calcination temperatures and times [6, 7, 15]. In this study, micron-sized hexagonal boron nitride was measured from the SEM image even at the shortest calcination time.

The raw material mixtures of all of the samples were prepared to obtain 30 wt% hBN. The quantitative amount of sintered sample phases was calculated by Rietveld analysis, and the results are given in Table 1. It was noticed that the amount of the hBN in the 4-h calcined sample was lower than that in the other samples. According to XRD graphs, boron oxide is present in the samples which were calcinated up to 12 h. As boron oxide was not taken into consideration in Rietveld analysis, the errors in phase quantities were accepted. Although boron oxide is neglected, it was found that the amount of hBN increases when the calcination time was more than 4 h. The calcination of the urea residues and/or multi-stage dehydration contribute to the formation of the boron nitride [45]. Therefore, the time of calcination is an important process parameter.

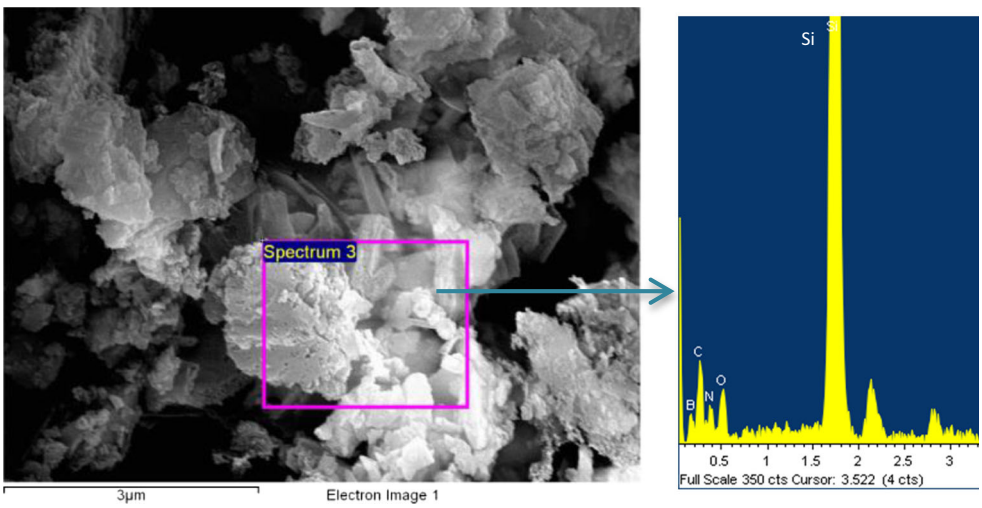

Fig. 5 EDS results of the S3-8 sample after calcination at 850 °C

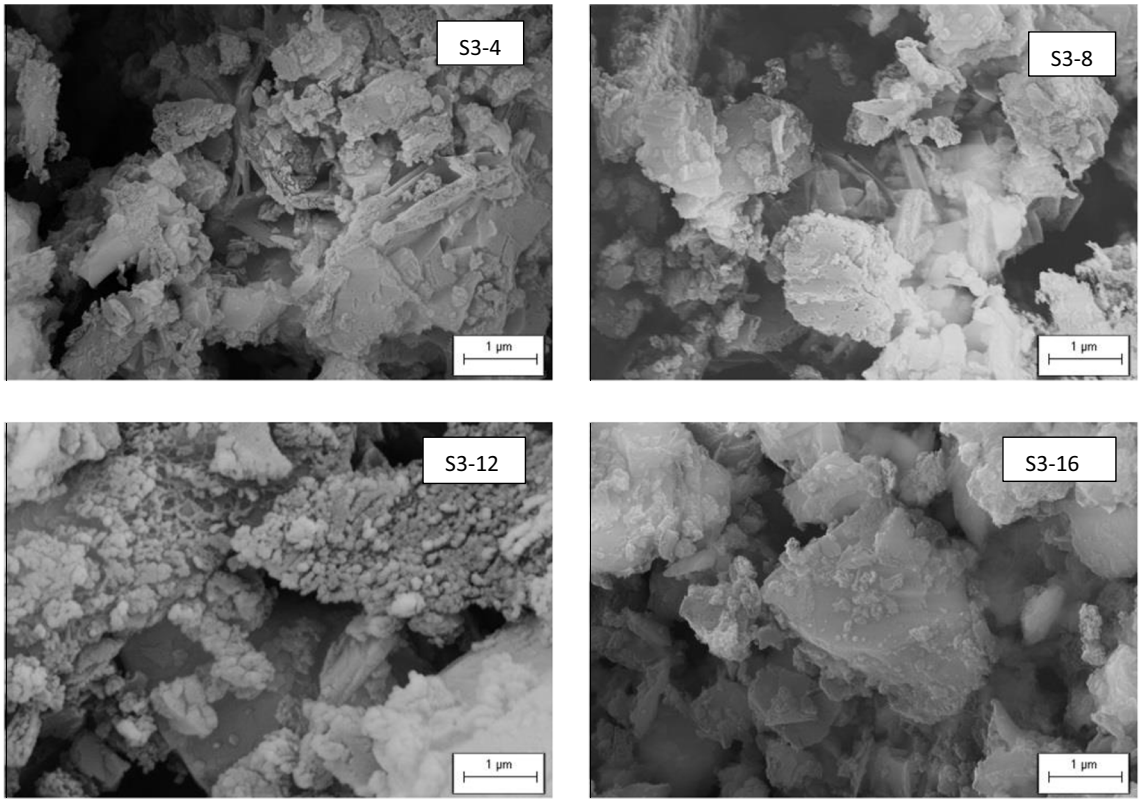

Fig. 6 SEM images of calcined samples at 850 °C

Densification behavior

Figure 10 shows the densification curves as a function of temperature and time for the hBN-SiC composite samples during the SPS process. The densification of the samples during sintering was determined by these curves depending on the amount of displacement in the punches. The relative piston movement exhibits the shrinking behavior in real-time densification of the powders. The initial densification temperatures of samples S3-4S, S3-8S, S3-12S, and S3-16S were 1987 °C, 1487 °C, 1449 °C, and 1404 °C, respectively. As the calcination time of the samples was increased, the initial temperature of the densification was decreased. Shuba and Chen have reported that the densification temperature is decreased with the addition of BN in an α-SiAlON/BN composite study [46]. In addition, in the study of Motealleh et al.

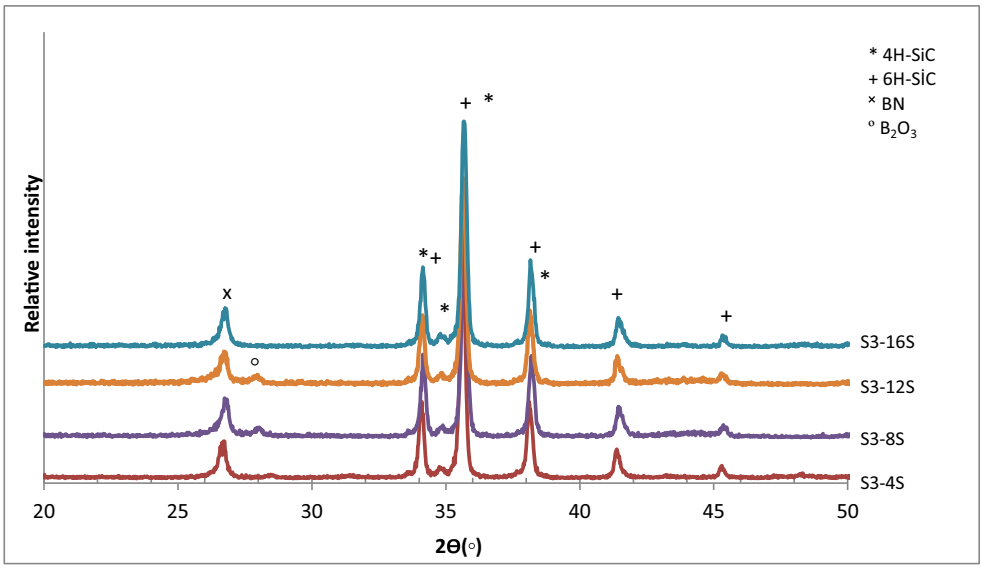

Fig. 7 XRD pattern of sintered samples at 2000 °C

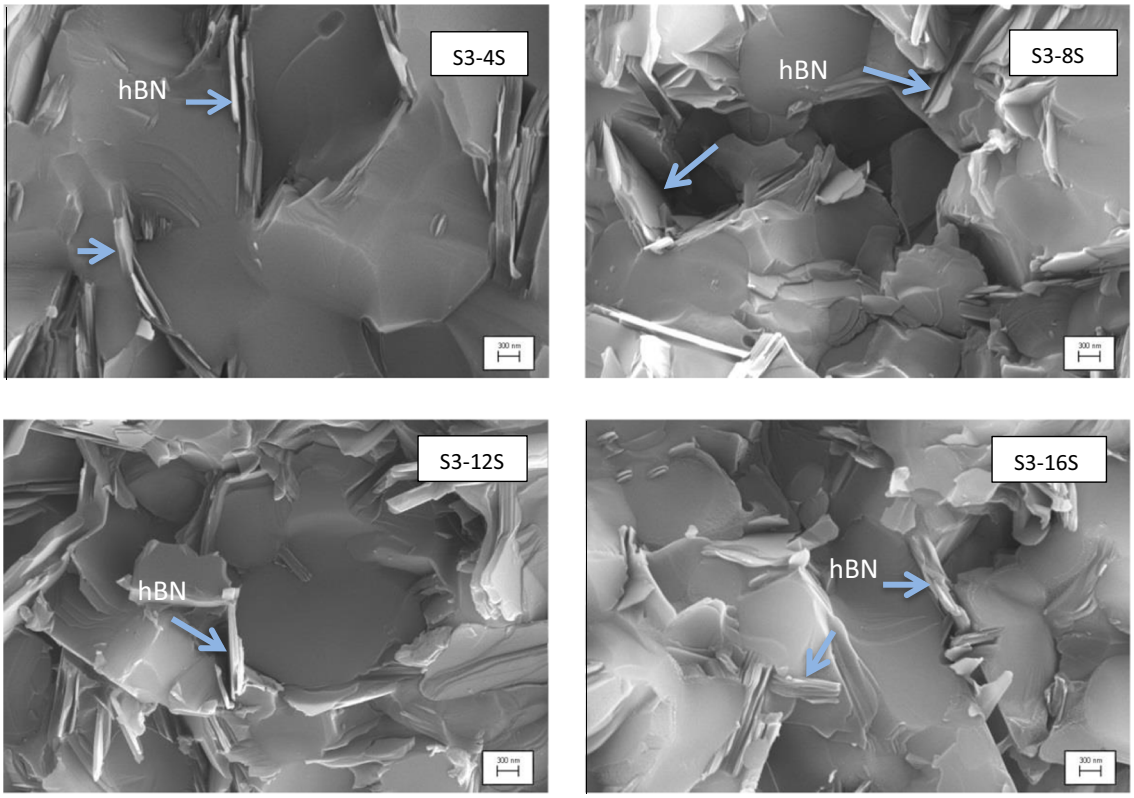

Fig. 8 SEM images of sintered samples at 2000 °C

which examined the wear behavior of SiC-hBN composites that were sintered by SPS using the liquid phase, it was shown that the densification curves decrease toward the lower temperatures with increasing the hBN content in the hBN-SiC composite [47]. In the S3-4S sample, densification continues during the sintering operation at 2000 °C for 15 min and it can be said that the densification has not been completed at the end of this period. It is impossible to sinter SiC intensively without any sintering additive. In various studies, SiC was produced by solid-state sintering at temperatures above 2200 °C with the addition of B and C at low ratios, and high-density SiC was produced at low temperatures between 1850 °C and 2000 °C using Al_2O_3 and Y_2O_3 sintering additives [48–50]. The shrinkage amounts from the densification beginning temperature to the end of the densification were calculated as 1.63 mm, 1 mm, 1.25 mm, and 2.28 mm for the samples S3-4S, S3-6S, S3-12S and S3-16S, respectively. When the sintering is examined from the beginning to the end of the S3-4S sample, it was determined that the amount of shrinkage is higher than that of the other samples. This shrinkage in the sample S3-4S depends on the excessive mass loss at sintering initial temperatures as a result of not completing the urea and

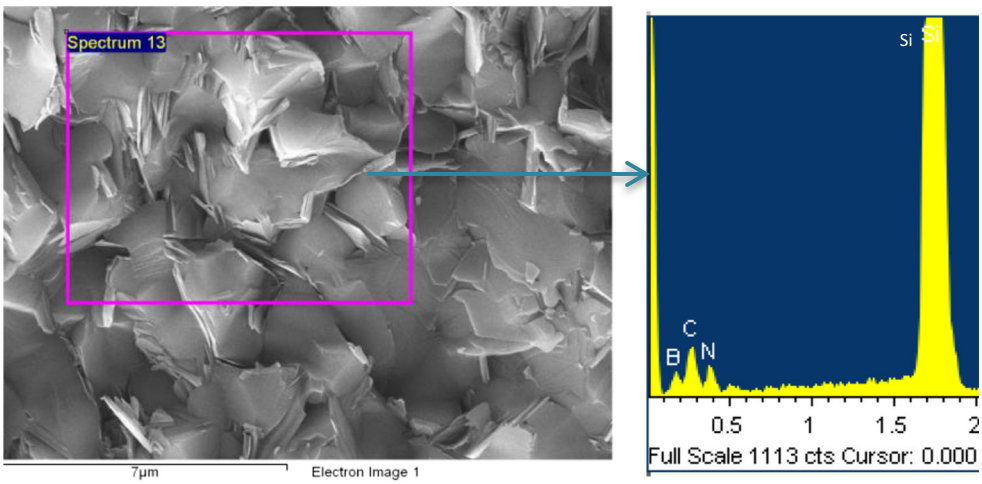

Fig. 9 EDS results of the sintered S3-16S sample at 2000 °C

Table 1 The amount of phases in the sintered samples

Sample code	6-h SiC wt%	4-h SiC wt%	Calculated hBN wt%	Theoretical hBN wt%
S3-4S	79.86	4.38	15.76	30
S3-8S	73.27	4.25	22.48	30
S3-12S	73.60	4.65	21.75	30
S3-16S	74.40	5.30	20.30	30

boric acid reactions during calcination, as shown in Fig. 2a. As the period of calcination increases, it is thought to be that the hBN particles which are located between the SiC grains, due to the high compaction pressures used in SPS, lead to a high rate at packing and thus an increase in shrinkage. This depicts that with the increasing calcination time, the hBN is better crystallized and consequently helps to pack at lower temperatures during sintering. In a study, it was reported that the hBN particles increased the packing amount and shortened intergranular diffusion distance. Furthermore, it has been reported that the hBN particles are very soft and compliant and therefore support packing as lubricants due to their deformations under high compaction pressures used in SPS [47]. Therefore, it can be considered that the hBN particles lubricate the SiC grains during the stage of mechanical compaction, thereby facilitating particle sliding and affecting packing.

Physical properties

The measurements of the physical properties of samples are given in Table 2. Silicon carbide has 347.01 GPa Young's modulus and 20–26 GPa hardness [51] while hBN has 36.5 GPa Young's modulus and 1–2 GPa hardness [52]. Therefore, hBN causes the reduction of Young's modulus and hardness in the composite material. It can be observed that the S3-4S sample has the lowest open porosity and the highest bulk density, but Young's modulus is the lowest among the samples. It was thought to be that the bulk density of this sample is higher due to impurities from precursor materials that are not incorporated into hBN during sintering. In the TG analysis of S3-4S, mass loss is the highest among the other samples. It is reported in literature that the addition of B and C is used for densification of silicon carbide, and B [53–56] and C [56] provide densification by increasing the diffusion at the SiC grain boundary. But the hardness measurement of S3-4S was not carried out because of collapsing. In addition, even though the same amount of calcined powder was utilized in all the samples during SPS, the S3-4S sample is the thinness sample. Some areas of the S3-4S sample have large pores that result in excessive gas exiting. For this reason, this sample has the lowest Young's modulus. After 8 h of calcination, the density of the samples increases with the extension of increasing calcination time. The results are in good agreement with shrinkage amount of the densification curves in the SPS. This presents that with increasing calcination time, the hBN is better crystallized and consequently helps to pack during sintering. Moreover, it is thought to be that the Vickers hardness values of all samples after 8 h of calcination reduce due to the increase in hBN [6, 15, 17] and better crystallization in the composite. Young's modulus increases slightly as the open porosity volume decreases. In addition, the study of SiC-hBN in which Yang et al. synthesized by an in situ method

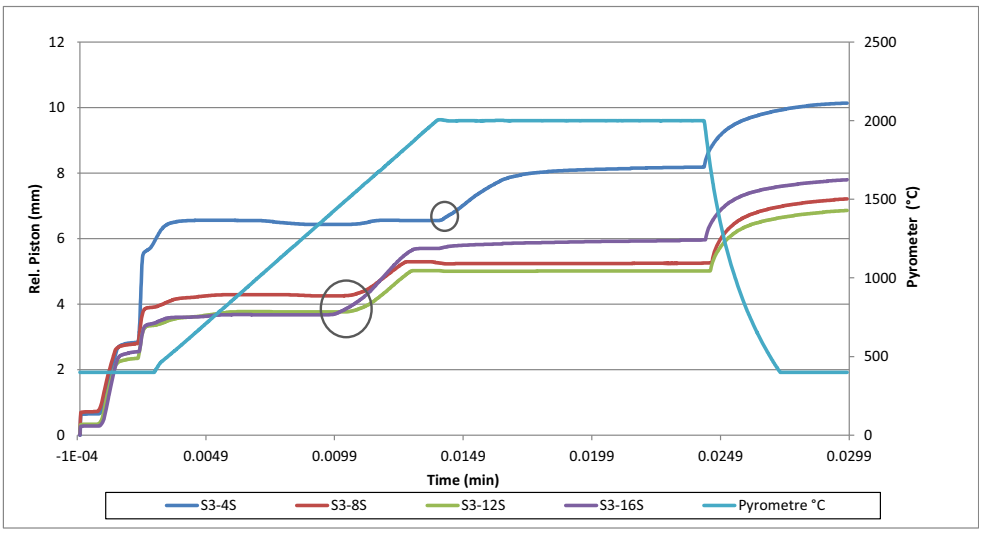

Fig. 10 SPS densification curves as a function of temperature and time

Table 2 The results of the physical properties of sintered samples at 2000 °C

Sample code	Open porosity (%)	Bulk density (g/cm^3)	Theoretical density (g/cm^3)	Relative density (%)	Young's modulus (*E*, GPa)	Vickers hardness (GPa)
S3-4S	2.963	2.875	3.062	93.89	122.266	Collapse
S3-8S	7.947	2.643	2.999	88.13	163.884	3.76
S3-12S	6.941	2.686	3.006	89.35	157.628	3.88
S3-16S	6.003	2.749	3.019	91.06	185.779	3.21

reported that Young's modulus decreased with increasing amount of hBN [57]. The amount of hBN in the S3-16S sample is less than those in the S3-8S and S3-12S samples, and Young's modulus is higher. Vickers hardness decreases in the S3-16S sample due to better crystallization of hBN in the composite. Due to the graphite-like layered crystal structure of hBN, the bond strength between the layers is low. Therefore, hBN is easily broken through the intermediate layers and this reduces the hardness of the composite.

Conclusions

The hBN-SiC composite was successfully produced by an in situ method using α-SiC, H_3BO_3, and $CO(NH_2)_2$, and calcination times on the hBN-SiC composite production were investigated at 850 °C. The following results can be drawn:

- Amorphous BN in the structure was formed when calcination was applied to composite powder mixtures at 850 °C, and it was found that phases and microstructure do not change with changing calcination time.
- As calcination time was increased, mass loss was decreased. The results indicated that reactions continued and calcination time must extend to minimum 12 h.
- The hBN structure was clearly confirmed after sintering at 2000 °C. The hBN is a flake shape and has been homogeneously formed at the grain boundaries of SiC.
- The hBN flakes in all the samples were measured for over 1 μm.
- Boron oxide remained in sintered samples which were calcined up to 12 h, and the calcination time caused to change the physical properties of the sintered samples.
- It has been concluded that the calcination period is an important process parameter in the production of the in situ hBN-SiC composite.

Funding information The authors would like to thank the Scientific Research Project Commission of Anadolu University (grant number 1406F321) for the financial support.

References

1. Abderrazak, H., Hadj Hmida, E.S.B.: Silicon carbide: synthesis and properties. In: Gerhardt, R. (ed.) Properties and Applications of Silicon Carbide, pp. 361–388. InTech, Tunisia (2011)
2. Rashed,A.H.: Properties and characteristics of silicon carbide. s.l.: Poco Graphite, TX. 76234, 1–19 (2002)
3. Saddow, S.E., Agarwal, A.: Advances in Silicon Carbide Processing and Applications, pp. 1–58053–1–740-5. Artech House, London (2004)
4. Shi, X., Wang, S., Yang, H., Duan, X., Dong, X.: Fabrication and characterization of hexagonal boron nitride powder by spray drying and calcining-nitriding technology. J. Solid State Chem. **181**, 2274–2278 (2008)
5. Ertuğ, B., Addemir, O.: Hegzagonal bor nitrür seramik tozlarının temel endüstriyel üretim yöntemleri. http://www.metalurji.org.tr/dergi/dergi136/d136_5458.pdf . Accessed 15 July 2017
6. Jin, H., Xu, H., Qiao, G., Gao, J., Jin, Z.: Study of machinable silicon carbide-boron nitride ceramic composites. Mater. Sci. Eng. A. 214–217 (2008)
7. Jin, H., Gao, N., Qiao, G., Gao, J.: Fabrication and properties of machinable SiC/h-BN nano-composites. J. Ceram. Process. Res. **9**, 630–633 (2008)
8. Zhang, G.J., Beppu, Y., Ohji, T., Kanzakı, S.: Reaction mechanism and microstructure development of strain tolerant in situ SiC–BN composites. Acta Mater. **49**, 77–82 (2000)
9. Zhang, G.J., Ohji, T.: Effect of BN content on elastic modulus and bending strength of SiC–BN in situ composites. Mater. Res. Soc. **15**, 1876–1880 (2000)
10. Zhang, G.J., Ohji, T.: In situ reaction synthesis of silicon carbide–boron nitride composites. J. Am. Ceram. Soc. **84**, 1475–1479 (2001)
11. Zhang, G.J., Yang, J.F., Deng, Z.Y., Ohjı, T.: Effect of Y_2O_3-Al_2O_3 additive on the phase formation and densification process of in situ SiC-BN composite. J. Ceram. Soc. Jpn. **109**, 45–48 (2001)
12. Zhang, G.J., Beppu, Y., Ando, M.: In situ reaction synthesis of silicon carbide–boron nitride composite from silicon nitride-boron oxide-carbon. J. Am. Ceram. Soc. **85**, 2858–2860 (2002)
13. Zheng, Y.T., Li, H.B., Zhou, T.: Microstructure and mechanical properties of h-BN–SiC ceramic composites prepared by in situ combustion synthesis. Mater. Sci. Eng. **A 540**, 102–106 (2012)
14. Kusunose, T., Sekino, T., Ando, Y.: Synthesis of SiC/BN nanocomposite powders by carbothermal reduction and nitridation of borosilicate glass, and the properties of their sintered composites. Nanotechnology. **19**, 275603 (2008) 9pp
15. Kusunose, T., Sekino, T., Niihara, K.: Contact damage of silicon carbide/boron nitride nanocomposites. J. Am. Ceram. Soc. **90**, 3341–3344 (2007)
16. Wang, X., Qiao, G., Jin, Z.: Preparation of SiC/BN nanocomposite powders by chemical processing. Mater. Lett. **58**, 1419–1423 (2004)

17. Wang, X., Qiao, G., Jin, Z.: Fabrication of machinable silicon carbide-boron nitride ceramic nanocomposites. J. Am. Ceram. Soc. **87**, 565–570 (2004)
18. Madhurambal, G., Mariappan, M., Mojumdar, S.C.: TG–DTA, UV and FTIR spectroscopic studies of urea-thiourea mixed crystal. J. Therm. Anal. Calorim. **100**, 853–856 (2010)
19. Jones, J.M., Rollinson, A.N.: Thermogravimetric evolved gas analysis of urea and urea solutions with nickel alumina catalyst. Thermochim. Acta. **565**, 39–45 (2013)
20. Chen, J.P., Isa, K.: Thermal decomposition of urea and urea derivatives by simultaneous TG/(DTA)/MS. J. Mass. Spectrom. Soc. Jpn. **46**, 299–303 (1998)
21. Sevim, F., Demir, F., Bilen, M., Okur, H.: Kinetic analysis of thermal decomposition of boric acid from thermogravimetric data. Korean J. Chem. Eng. **23**, 736–740 (2006)
22. Gedikbey, T., Şarda, D., Birlik, E.: Uleksit ve tünellit mineralinden borik asit üretimi. IIUluslararasi Bor Sempozyumu. 291–296 (2004)
23. Condon, J.B., Holcombe, C.E., Johnson, D.H., Steckel, L.M.: The kinetics of the boron plus nitrogen reaction. Inorg. Chem. **15**(9), 2173–2179 (1976)
24. Besisaa, D.H.A., Hagrasa, M.A.A., Ewaisa, E.M.M., Ahmeda, Y.M.Z., Zakia, Z.I., Ahmed, A.: Low temperature synthesis of nano-crystalline h-boron nitride from boric acid/urea precursors. J. Ceram. Process. Res. **17**, 1219–1225 (2016)
25. Berchmans, L.J., Bharathi, B., Amalajyothi, K., Subramanian, K.: Synthesis of nanocrystalline boron nitride by combustion process. Int. J. Self-Propag. High-Temp. Synth. **18**, 34–37 (2009)
26. Tehrani, F.S., Goh, B.T., Muhamad, M.R., Rahman, S.A.: Pressure dependent structural and optical properties of silicon carbide thin films deposited by hot wire chemical vapor deposition from pure silane and methane gases. J. Mater. Sci. Mater. Electron. **24**, 1–8 (2012)
27. Saravanan, L., Subramanian, S., Vishu Kumar, A.B., Tharanathan, R.N.: Surface chemical studies on SiC suspension in the presence of chitosan. Ceram. Int. **32**, 637–646 (2006)
28. Garbuz, V.V., Lobunets, T.F., Petrova, V.A., Tomila, T.V., Suvorova, L.S.: Physicochemical characterstics of nitrogen sorption on high-porous powders of graphene-like boron nitride powder. Metall. Met. Ceram. **55**, 7–8 (2016)
29. Lopes, B.B., Rangel, R.C.C., Antonio, C.A., Durrant, S.F., Cruz, N.C., Rangel, E.C.: Mechanical and tribological properties of plasma deposited a-C:H:Si:O films, Nanoindentation in Materials Science, Chapter 8. J. Nemecek. 170–202 (2012)
30. Rashid, N.M.A., Ritikos, R., Goh, B.T., Gani, S.M.A., Muhamad, M.R., Rahman, S.A.: Effects of thermal annealing on the properties of highly reflective nc-Si:H/a-CNx:H multilayer films prepared by r. f. pecvd technique. Solid State Sci. Technol. **19**, 132–137 (2011)
31. Bondareva A.V., Kovalskiia A.M., Firesteina K.L., Loginova B P.A., Sidorenkoa D.A., Shvindinaa N.V., Sukhorukovaa I.V., Shtanskya D.V.: Hollow spherical and nanosheet-base BN nanoparticles as perspective additives to oil lubricants: correlation between large-scale friction behavior and in situ TEM compression testing. Ceram. Int. **44**, 6801–6809 (2018)
32. Kharazmi, A., Faraji, N., Hussin, R.M., Saion, E., Mat Yunus, W.M., Behzad, K.: Structural, optical, opto-thermal and thermal properties of ZnS–PVA nanofluids synthesized through a radiolytic approach. J. Nanotechnol. **6**, 529–536 (2015)
33. Fischer P.H.H., McDowell C.A: The infrared absorption spectra of urea-hydrocarbon. Can. J. Chem. 38, (1960)
34. Renuga Devı, T.S., Gayathrı, S.: FTIR and FT-Raman spectral analysıs of paclitaxel drugs. Int. J. Pharm. Sci. Rev. Res. **2**, 106–110 (2010)
35. Burie, J.R., Boussac, A., Bodlais, C., Berger, C., Mattioli, T., Mioskowski, C., Nabedryk, E., Breton, J.: FTIR spectroscopy of uv-generated quinone radicals: evidence for an ıntramolecular hydrogen atom transfer in ubiquinone, naphthoquinone and plastoquinone. J. Phys. Chem. **99**, 4059–4070 (1995)
36. Grdadolnik, J., Maréchal, Y.: Urea and urea–water solutions an infrared study. J. Mol. Struct. **615**, 177–189 (2002)
37. Hernandez, M.T., Gonzalez, M.: Synthesis of resins as alpha-alumina precursors by the Pechini method using microwave and infrared heating. J. Eur. Ceram. Soc. **22**, 2861–2868 (2002)
38. Oancea, A., Grasset, O., Le Menn, E., Bollengier, O., Bezacier, L., Le Mouélic, S., Tobie, G.: Laboratory infrared reflection spectrum of carbon dioxide clathrate hydrates for astrophysical remote sensing applications. Icarus. **221**, 900–910 (2012)
39. Kodera, Y., Toyofuku, N., Yamasaki, H., Ohyanagi, M., Munir, Z.A.: Consolidation of SiC/BN composite through MA-SPS method. J. Mater. Sci. **43**, 6422–6428 (2008)
40. Akyol, S., Toy, C., Gönül, T., Tekin, A.: Crystallization behavior and characterization of turbostratic boron nitride. J. Eur. Ceram. Soc. **17**, 1415–1422 (1997)
41. Hagıo, T., Nonaka, K., Sato, T.: Microstructural development with crystallization of hexagonal boron nitride. J. Mater. Sci. Lett. **16**, 795–798 (1997)
42. Thomas, J., Weston, N.E., O'Connor, T.E.: Turbostratic boron nitride, thermal transformation to ordered-layer-lattice boron nitride. J. Am. Chem. Soc. **84**, 4619–4622 (1963)
43. Hubáček, M., Ueki, M., Sato, T., Brozek, V.: High-temperature behaviour of hexagonal boron nitride. Thermochim. Acta. **282/283**, 359–367 (1996)
44. Brožek, V., Hubáček, M.: A contribution to the crystallochemistry of boron nitride. J. Solid State Chem. **100**, 120–129 (1992)
45. Garbuz, V.V., Petrova, V.A., Suvorova, L.S., Silinska, T.A., Kuzmenko, L.M.: Model of reactions for the synthesis of turbostratic boron nitride nanoparticles from urea. Powder Metall. Met. Ceram. **56**, 7–8 (2017)
46. Shuba, R., Chen, I.-W.: Machinable α-SiAlON/BN composites. J. Am. Ceram. Soc. **89**, 2147–2153 (2006)
47. Motealleh, A., Ortiz, A.L., Borrero-López, O., Guiberteau, F.: Effect of hexagonal-BN additions on the sliding-wear resistance offine-grained alpha-SiC densified with $Y_3Al_5O_{12}$ liquid phase by spark-plasma sintering. J. Eur. Ceram. Soc. **34**, 565–574 (2014)
48. Abderrazak, H., Hadj Hmida, E.S.B.: Silicon carbide: synthesis and properties. R. Gerhardt. Properties and Applications of Silicon Carbide. Tunisia: InTech, 3, 201161–388 (n.d.)
49. Omori, M., Takei, H.: Pressureless sintering of SiC. J. Am. Ceram. Soc. **65**, 92 (1982)
50. She, J.H., Ueno, K.: Effect of additive content on liquid-phase sinterıng on silicon carbide ceramics. Mater. Res. Bull. **34**, 1629–1636 (1999)
51. Luoa, X., Goel, S., Reuben, R.L.: A quantitative assessment of nanometric machinability of major polytypes of single crystal silicon carbide, s.l. J. Eur. Ceram. Soc. **32**, 3423–3434 (2012)
52. Kumar, V.: Synthesis and study of photoluminescence properties of nanostructured boron nitride, pp. 44–50. Jadavpur University, India (2011)
53. Lorrette, C., Réau, A., Briottet, L.: Mechanical properties of nanostructured silicon carbide consolidated by spark plasma sintering. J. Eur. Ceram. Soc. **33**, 147–156 (2013)
54. Maıtre, A., Vande Put, A., Laval, J.P., Valette, S., Trolliard, G.: Role of boron on the spark plasma sintering of an alfa-SiC powder. J. Eur. Ceram. Soc. **28**, 1881–1890 (2008)
55. Stobierski, L., Gubernat, A.: Sintering of silicon carbide II. Effect of boron. Ceram. Int. **29**, 355–361 (2003)
56. Lu, B., Zhang, Y.: Densification behavior and microstructure evolution of hot-pressed SiC–SiBCN ceramics. Ceram. Int. **4**, 8541–8551 (2015)
57. Yang, Z.H., Jia, D.C., Zhou, Y., Shi, P.Y., Song, C.B., Lin, L.: Oxidation resistance of hot-pressed SiC–BN composites. s.l. Ceram. Int. **34**, 317–321 (2008)